

Sticky-Glance: Robust Intent Recognition for Human Robot Collaboration via Single-Glance

Yuzhi Lai¹, Shenghai Yuan², Peizheng Li^{1,3} and Andreas Zell¹

Abstract—Gaze is a valuable means of communication for impaired people with extremely limited motor capabilities. However, robust gaze-based intent recognition in multi-object environments is challenging due to gaze noise, micro-saccades, viewpoint changes, and dynamic objects. To address this, we propose an object-centric gaze grounding framework that stabilizes intent through a sticky-glance algorithm, jointly modeling geometric distance and direction trends. The inferred intent remains anchored to the object even under short glances with minimal 3 gaze samples, achieving a tracking rate of 0.94 for dynamic targets and selection accuracy of 0.98 for static targets. We further introduce a continuous shared control and multi-modal interaction paradigm, enabling high-readiness control and human-in-loop feedback, thereby reducing task duration for nearly 10 %. Experiments across dynamic tracking, multi-perspective alignment, a baseline comparison, user studies, and ablation studies demonstrate improved robustness, efficiency, and reduced workload compared to representative baselines.

I. INTRODUCTION

Gaze provides a direct, low-effort channel to express intent, and has long served as an input modality in robot teleoperation [1] and robotic manipulation [2], [3]. This capability becomes mission-critical in assistive robotics for users with severe motor impairments (e.g., upper-limb disability), who often retain intact cognition and voluntary eye movements [4]. In this setting, a practical gaze interface must do more than decode where the user looks: it must reliably infer object-level intent in real time, under natural head/eye motion and cluttered scenes, while supporting safe and efficient human-in-the-loop control.

The **existing** gaze-intent pipelines are biased toward either temporal persistence or statistical smoothing in gaze space, which makes them brittle in realistic, dynamic environments [5]. Prolonged-fixation designs trade responsiveness for stability and can still break under jitter and transient glances [6]. Distribution-based approaches reduce noise but often ignore object-centric geometric consistency and explicit temporal constraints [7]. Probabilistic models improve interpretability yet typically rely on delicate parameter tuning and manually specified transitions that do not transfer cleanly across users and scenes [2], [8]. Purely data-driven solutions require extensive labeled data and often generalize poorly when users, viewpoints, or object layouts change. Beyond intent

Corresponding Author: **Andreas Zell**. This work was supported in part by Meta, and we acknowledge their contribution of Meta Glasses for this research.

¹University of Tuebingen, Geschwister-Scholl-Platz, 72074 Germany, {name.surname}@uni-tuebingen.de.

²Nanyang Technological University, 50 Nanyang Avenue, Singapore 639798, shyuan@ntu.edu.sg.

³peizheng.li@mercedes-benz.com.

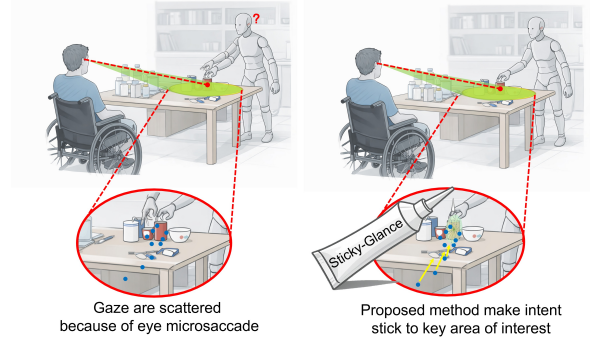


Fig. 1. Our proposed approach anchors scattered gaze points to intent objects, enabling efficient and natural interaction with a short glance.

recognition, many gaze-driven robotic systems still operate with a discrete target-pose triggering controller, offering limited continuous feedback during intent formation and thus constraining responsiveness and interaction quality in assistive use [3], [6].

The core **challenge** is a tripartite coupling of (i) noisy, nonstationary gaze trajectories (micro-saccades, head motion), (ii) multi-object dynamics and viewpoint changes that make gaze-to-object grounding ambiguous, and (iii) control requirements that demand both stability (avoid unintended selection) and immediacy (avoid long dwell times). Solving only the perception side (denoising gaze) is insufficient if the downstream interaction remains discrete and non-responsive; conversely, improving control without robust object-level intent grounding leads to unsafe or frustrating operation.

To address these challenges, we propose an object-centric gaze grounding and interaction framework that stabilizes intent directly in geometric space rather than solely in gaze perspective. Instead of relying on prolonged fixation or purely probabilistic belief propagation, we accumulate geometric and temporal evidence by jointly modeling distance and directional trends of gaze motion. This allows intent to “stick” to object regions even under short glances and dynamic conditions. Building on this stabilized intent signal, we further introduce a continuous joint controller and interaction paradigm that couples gaze-based object selection with speech-based action specification. It synthesizes (i) a virtual target anchored to grounded objects and (ii) a gaze-conditioned velocity field. Unlike conventional target-pose triggering, our system provides continuous motion feedback and slow-following during intent formation, enabling more responsive and efficient gaze-driven HRI.

Our main contributions are summarized below:

- We propose a gaze grounding and sticky intent stabilization module that maps noisy gaze to object-centric intent, maintaining robust target assignment under micro-saccades and dynamic object motion without prolonged fixation, per-task fine tuning or initialization, achieving a tracking rate of 0.94 for dynamic targets and a selection accuracy of 0.98 for static targets.
- We introduce a continuous control strategy that modulates motion generation based on gaze confidence and spatial proximity, transitioning between standby behavior and rapid attraction to enhance efficiency and predictability, reducing task duration for nearly 10 %.
- We implement a gaze-speech interaction protocol (“glance-say”) leveraging continuous gaze for target grounding and discrete speech for execution, with an explicit confirmation step for interaction safety. Extensive experiments across dynamic tracking, multi-perspective alignment, and user studies demonstrate improved robustness, efficiency, and usability in multi-object manipulation scenarios. While ensuring the highest success rate (0.96), it also achieves the lowest cognitive load (25.57) and usability evaluation (86.42).

II. RELATED WORKS

A. Gaze-based Intent Recognition

The goal of gaze-based intent recognition is to infer which object a user intends to interact with based on gaze signals. Existing approaches can be broadly categorized into model-based, learning-based, distribution-based, and fixation-based.

Model-based approaches formulate intent prediction as a sequence modeling or classification problem using Hidden Markov Models (HMMs) [2], [8], Support Vector Machines (SVMs) [9], or Partially Observable Markov Decision Process (POMDP) [10]. Some researchers also utilized learning-based methods such as Recurrent Neural Networks (RNNs) [11] or Long Short-Term Memory (LSTM) [12]. These methods analyze gaze trajectories within a temporal window and output the most likely selected object. While capable of modeling temporal dependencies, they typically require large labeled datasets, are sensitive to time window selection, and involve complex parameter tuning. In practice, performance varies across users and environments, limiting robustness and real-world scalability. TAGMM [13] models gaze dynamics using a Kalman filter with an artificial attractor field, assuming that gaze trajectories follow a physically driven acceleration toward the intended target. However, human gaze behavior does not strictly obey such deterministic attractor dynamics. Moreover, the model requires 800 ms of gaze history for initialization and parameter stabilization, introducing a non-negligible latency in interaction system. Distribution-based methods estimate intent by aggregating gaze samples over time, such as through clustering [7], weighted trajectory accumulation [3], or spatial probability modeling [14]. Although they reduce reliance on labeling data, they operate primarily in gaze space and do not explicitly model motion

trends or geometric constraints between gaze trajectories and object. The most widely adopted strategies rely on fixation or dwell-time thresholds [6], [15], where an object is selected only when a sufficient number of gaze samples fall within its region. While simple and easy to implement, these approaches require prolonged fixation and are sensitive to natural micro-saccades. In static scenes, involuntary gaze jitter may cause gaze points to drift outside object boundaries, leading to selection failure. In dynamic scenes, tracking performance further degrades because sustained fixation on moving objects becomes difficult. A degenerate case of this strategy reduces selection to the last gaze point with a k-Nearest Neighbor-based (kNN) approach [16], [17]. Such approaches are highly sensitive to noise, as a single noise gaze sample lead to incorrect prediction.

B. Gaze-Based Interaction & Control Strategies

Existing gaze-based robotic interaction strategies can be broadly categorized into interface-centric control [1], [15], [16], and multi-modal interaction [3].

Interface-centric approaches rely on gaze-controlled graphical user interfaces (GUI). In GazeWheelChair [4], researchers designed an interface integrated with the wheelchair, allowing users to teleoperate the robot arm step by step via gaze selection on the screen. Similarly, FreeView [1] introduced a virtual interface anchored around the robot end-effector, where users operate the manipulator by fixating on interactive elements positioned near the tool. While these methods provide explicit and precise control, users must continuously attend to interface elements, resulting in long command duration, high cognitive load, and considerable learning cost [18]. To reduce complexity, MR-GUI [15] simplifies the interaction by allowing users to first select an object through gaze and then choose the desired action via a GUI. Although this design shortens command duration compared to full teleoperation interfaces, it still relies on GUI elements, constraining interaction to predefined interface locations and limiting flexibility in dynamic environments. In contrast, GlanceGaze [6] removes the explicit GUI by leveraging a vision-language model (VLM) to infer the intended action directly from gaze and scene context. In [19], similarly, researchers utilize gaze and LSTM to infer action primitives and target pose. However these action inference is unreliable in ambiguous scenarios (e.g., distinguishing between “put” and “pour”), affecting task stability and success rate. Multi-modal approaches, such as FAM-HRI [3] and HIP-HRI [16], combine gaze for object selection with speech for action specification. These methods integrate the advantages of both modalities, reducing ambiguity and lowering cognitive load compared to GUI-based approaches.

However, despite improved interaction efficiency, these systems predominantly adopt a target-pose control paradigm, where robot motion is triggered only after intent confirmation and pose determination. Consequently, they lack continuous motion feedback and do not provide pre-alignment behavior during intent formation.

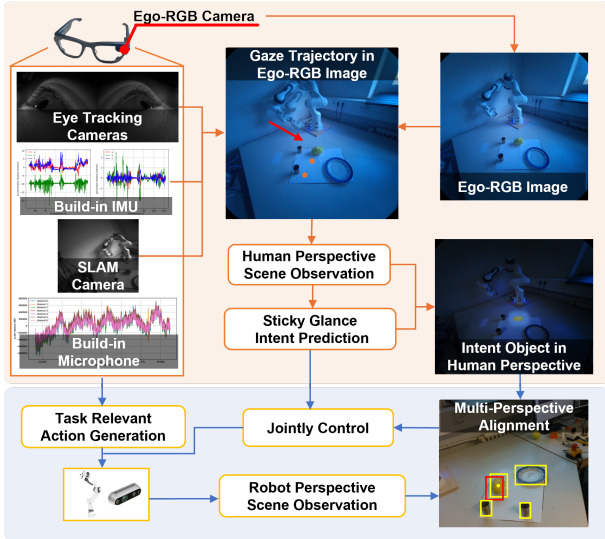


Fig. 2. Our system collects data through Meta ARIA glasses, then performs asynchronous off-device inference. Data is transmitted via Wi-Fi.

III. METHODOLOGY

A. Problem Formulation

We consider the problem of inferring object-level user intent from noisy and unstable gaze points $g(t) \in \mathbb{R}^2$ with respect to time t in a 3D robotic workspace containing candidate objects $\mathcal{Z}_i \in \mathbb{R}^3$. The objective is to reliably infer the intended object $\mathcal{Z}_{i^*} \in \mathbb{R}^3$ from gaze points, such that stable intent can be established through a short glance despite gaze noise, user motion, and object motion. Once intent is inferred, the robot immediately begins moving toward the corresponding object. Our system is shown in Fig. 2.

B. Human Perspective Perception

1) *Gaze Trajectory Projection*: We utilize Meta ARIA glasses and their built-in eye tracking cameras to obtain per-frame gaze points in the ego-image [20]. The built-in SLAM camera and IMU are utilized to estimate camera poses. The gaze point from previous frame $g(t-1)$ is then reprojected into the current frame of the ego-image to obtain the gaze trajectory with current gaze point $g(t)$ as shown in Fig. 3.

2) *Human Perspective Scene Observation*: A fine-tuned YOLO26 [21] is used for object detection, and ByteTrack [22] is employed for multi-object tracking in the ego-RGB images. To robustly handle object shape variations, objects with an aspect ratio of their bounding box smaller than 2:1 are approximated by a single circumscribed circle centered at the bounding box center. For elongated objects with an aspect ratio larger than 2:1, we divided the bounding box based on the shorter side's length and place multiple circumscribed circles along the principal axis of the bounding box, which are generally referred to as objects for simplification.

C. Sticky-Glance Intent Prediction Algorithm

The goal of the sticky-glance algorithm is to construct an object-centric confidence field in which candidate objects

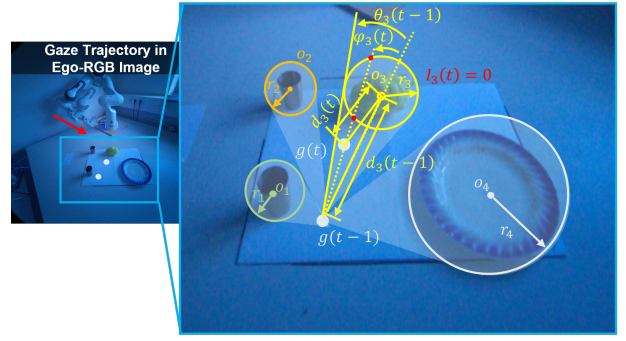


Fig. 3. Illustration of the gaze trajectory (left) and the calculation for Sticky-Glance Intent Prediction (right).

generate attraction or repulsion toward gaze motion, enabling stable and geometrically grounded intent assignment.

As shown in Fig. 3, each candidate object $\{\mathcal{H}_i\}_{i=1}^N$ is represented by a circular region centered at o_i with expanded radius r_i from the detected circumscribed circle (from Sec. III-B) to tolerate gaze noise and detection results. As shown by the light blue cone in Fig. 3, we further define a tangent cone for each object \mathcal{H}_i . This cone is formed by the two tangent lines from the previous gaze point $g(t-1)$ with \mathcal{H}_i .

We first define the distance between the gaze point and object center as: $d_i(t) = \|g(t) - o_i\|_2$, and the distance trend as: $\sigma_i(t) = \text{sgn}(d_i(t-1) - d_i(t))$, which indicates whether the gaze is moving toward or away from the object. Based on this, we further define a distance-evidence term:

$$e_i^{\text{dist}}(t) = \begin{cases} 1, & d_i(t) \leq r_i \\ (1 - \frac{d_i(t) - r_i}{d_i(t)})\sigma_i(t), & \text{Otherwise} \end{cases} \quad (1)$$

When the current gaze lies inside the object region, $e_i^{\text{dist}}(t)$ is set to 1, indicating strong intent assignment. Otherwise, the confidence is modulated by the trend $\sigma_i(t)$, increasing when gaze approaches the object and vice versa. This formulation ensures bounded evidence in $[-1, 1]$.

By leveraging the tangent cone, we define the directional trend of the gaze. The cone represents the feasible angular region within which gaze motion would intersect or approach the object. The cone boundary angle $\theta_i(t-1)$ is determined by the object geometry and the gaze-object distance, with $\cos \theta_i(t-1) = \sqrt{1 - (\frac{r_i}{d_i(t-1)})^2}$, which defines the angular limit of object-directed motion. The actual gaze motion direction is represented by the angle $\varphi_i(t)$ between the gaze displacement vector $g(t) - g(t-1)$ and the object direction vector $o_i - g(t)$ as $\cos \varphi_i(t) = \frac{(g(t) - g(t-1)) \cdot (o_i - g(t))}{\Delta g(t) d_i(t)}$, where $\Delta g(t) = \|g(t) - g(t-1)\|_2$. If the gaze motion lies inside the tangent cone, the gaze is moving toward the object; otherwise, it is diverging. Based on this geometric relationship, the direction evidence of the confidence field is defined as:

$$e_i^{\text{dir}}(t) = \begin{cases} -1, & I_i(t) = 2 \\ \frac{\cos \varphi_i(t) - \cos \theta_i(t-1)}{1 - \delta_i(t) \cos \theta_i(t-1)}, & \text{Otherwise} \end{cases} \quad (2)$$

We define $I_i(t)$ as the number of intersection points between the gaze displacement vector $g(t) - g(t-1)$ and the circular

Algorithm 1 Sticky-Glance Intent Prediction

Input: Objects $\{\mathcal{H}_i = (o_i, r_i)\}_{i=1}^N$, gaze $\{g(t)\}_{t=0}^T$
Output: Confidence $\mathbf{c}(t, i) \in [0, 1]^N$, list of intent i^*
Parameter: Saccade threshold τ , Step Δt , Threshold c_{min}

```

1: for  $i = 1$  to  $N$  do
2:    $e_i^{dist} \leftarrow 0, e_i^{dir} \leftarrow 0$ 
3:   if  $d_i(t-1) > r_i \wedge \Delta g(t) > \tau$  then
4:      $e_i^{dist}, e_i^{dir} \leftarrow$  Eq. 1, 2
5:   else if  $d_i(t-1) \leq r_i$  then
6:     if  $d_i(t) \leq r_i \vee \Delta g(t) < \tau$  then
7:        $e_i^{dist} \leftarrow 1$   $\triangleright$  Fixation on object
8:     else if  $d_i(t) > r_i$  then
9:        $e_i^{dir} \leftarrow -1, e_i^{dist} \leftarrow$  Eq. 1
10:    end if
11:  end if
12:   $e_i \leftarrow e_i^{dist} + e_i^{dir}$ 
13:   $\mathbf{c}(t, i) \leftarrow \text{clip}(\mathbf{c}(t-1, i) + \Delta t \cdot e_i, 0, 1)$ 
14:  if  $\mathbf{c}(t, i) \geq c_{min}$  then
15:     $i^*.append(i)$   $\triangleright$  Intent Update
16:  else
17:     $i^* \leftarrow i^*$   $\triangleright$  No selection
18:  end if
19: end for
  
```

region \mathcal{H}_i . If $I_i(t) = 2$, the gaze trajectory has already passed through the object, indicating divergence from the object, so the $e_i^{dir} = -1$. We also define $\delta_i(t) = \text{sgn}(\cos \varphi_i(t) - \cos \theta_i(t-1))$ to normalize e_i^{dir} , ensuring values in $[-1, 1]$.

Our proposed sticky-glance algorithm updates the confidence for each object over time using e_i^{dir} and e_i^{dist} . As shown in Alg. 1, we first distinguish glance from fixations using the threshold τ . The per-object confidence is then integrated over time and clipped to $[0, 1]$, ensuring bounded and stable intent. The object is selected as the intended target when $\mathbf{c}(t, i) \geq c_{min}$; otherwise, no object is selected. This object-centric confidence field employs integral updates to induce a “sticky” effect, anchoring intent to targets. The field also acts as an attractive–repulsive mechanism, accelerating confidence growth for valid gaze motions while rapidly suppressing invalid. This mechanism filters transient micro-saccades while enabling seamless intent switching only upon sufficient directional and spatial evidence accumulation.

D. Robot Perspective Perception

1) *Object Level Pointcloud Association:* To avoid information loss from a single viewpoint and safe motion planning, we constructed complete object-level point clouds. Based on prior work [23], we optimize object-level association via a robot-mounted RGB-D camera (Fig. 4). The system explores the workspace, aligning and merging captured point clouds through Iterative Closest Point (ICP) registration to generate object-level representations. iForest isolation is applied to remove the background and to ensure a smooth object geometry \mathcal{Z}_i . We then construct a topology graph,

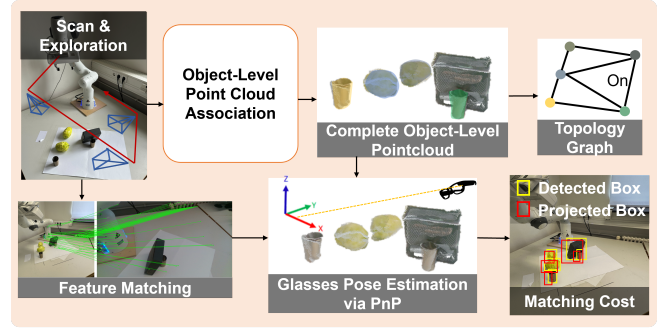


Fig. 4. Demonstration of the pipeline for object-level pointcloud association and the pipeline for multi-perspective alignment.

where each node represents an object with its semantic label (from Sec. III-B.2), 3D position, and pre-grasping pose [24] (above the object). Edges encode spatial relations: “on” if vertical projections overlap, and “in” if horizontal projections are enclosed.

2) *Multi-Perspective Alignment:* To enable the robot to identify the object intent object, multi-perspective alignment between the human and robot perspectives is required. Previous feature-based voting alignment [3], [6] often fails due to insufficient matching of object features and misdetection of ArUco markers. As shown in Fig. 4, we propose an optimal matching based method. We first perform feature matching using LightGlue [25] (most matched points are from the background) and estimate the ego-RGB camera pose via Perspective-n-Point (PnP). Using this pose, 3D object point clouds (from Sec. III-D.1) are projected into the ego-RGB image to obtain normalized projected bounding boxes $b_m^p = [\frac{x_m}{W}, \frac{y_m}{H}, \frac{w_m}{W}, \frac{h_m}{H}]$, where W, H represent the width and height of the ego-RGB image. With normalized detected boxes b_n^d from Sec. III-B.2, we define the cost:

$$L = \|b_m^p - b_n^d\|_2 \quad (3)$$

where m and n represent the index of the bounding box. To ensure reliable associations, candidate pairs are pre-filtered using an IoU threshold ($\text{IoU} > 0.6$) [23]. The Hungarian algorithm is applied to obtain optimal object correspondence with minimal L . To ensure real-time performance, multi-view alignment is only performed at the start of interaction (first frame) and when new objects appear. For failure treatment, please refer to Sec. III-E.

E. Continuous Shared Control and Interaction

Continuous robot response is critical for intuitive interaction, as delayed or unstable motion can degrade usability and safety. During the confidence updating and intent transitions, multiple candidate objects may temporarily exhibit high confidence. To ensure smooth and predictable behavior, we define a confidence-weighted virtual target as:

$$\mathcal{P}(t, i^*) = \frac{\sum_{i^*} (\mathbf{c}(t, i^*) \mathcal{P}_g^{i^*})}{n} \quad (4)$$

Here n denotes the number of intended objects, and $\mathcal{P}_g^{i^*}$ denotes the pre-grasping position, which is decomposed from

pre-grasp pose $\mathcal{T}_g^{i^*}$ (see Sec. III-D.1). We also define two control modes: a pre-command mode for continuous standby and a post-command mode for task execution.

Prior to the user providing an explicit task command through speech, the robot operates in pre-command mode. The angular velocity is defined as $\omega_{pre}(t) = 0$ and the linear velocity is defined as:

$$v_{pre}(t) = \underbrace{\sum_{i^*} (c(t, i^*) v_{max})}_n \sigma_e(t, i^*) u(t, i^*) \quad (5)$$

Where $v(t, i^*)$ is a confidence-weighted velocity that increases with confidence. $\sigma_e(t, i^*) = \text{clip}(\frac{\mathcal{P}^e(t) - \mathcal{P}(t, i^*)}{\Delta R}, 0, 1)$ modulates the velocity based on the distance to the target, reducing speed when approaching a predefined safety distance ΔR to ensure smooth deceleration. The unit vector $u(t, i^*) = \frac{\mathcal{P}(t, i^*) - \mathcal{P}^e(t)}{\|\mathcal{P}(t, i^*) - \mathcal{P}^e(t)\|_2}$ defines the motion direction from the current end-effector position $\mathcal{P}^e(t)$ to the virtual target.

Upon detecting a speech command, the system switches to post-command mode and commits to a single intended object. The index of the intended object i_m is selected as $i_m = \arg \max_{i^*} (c(t, i^*))$, which resolves the virtual target to a real target. In post-command mode, the robot moves towards the intended object with maximum velocity while ensuring safe approach and then aligns its orientation with the pre-grasp orientation [26].

$$v_{post}(t) = v_{max} \sigma_e(t, i_m) u(t, i_m) \quad (6)$$

To avoid interaction failures caused by intent recognition algorithms and multi-view matching, after reaching the target, the robot pauses and waits for user confirmation via speech. If the user confirms, the corresponding object is selected as the intended object $\mathcal{Z}_{i^*}(t)$ and the robot proceeds with task execution. If the user rejects the selection, the robot moves to the object with the second high confidence with Eq. 6, repeat the confirmation process. If the user rejects again, the robot returns to its initial pose, re-inferences and waits for the next user intent. This confirmation mechanism ensures safe and reliable interaction while allowing directly correction of intent. To ensure safety, the robotic arm's end effector is positioned above all objects, with a maximum speed of 10 cm/s and we set ΔR as 5 cm.

F. Task Relevant Action Generation

To enable real-time task planning from speech and glance, we followed the previous approaches [27]. The speech command is encoded using a BGE model [28] and matched with action primitives based on similarity. The primitives include *pick*, *put*, *pour*, *swap*, *grasp*, *push*, *move* and *rotate*.

The selected action is executed using a behavior tree planner integrated with the topology graph, enabling topology-aware manipulation. This allows the system to automatically generate intermediate actions, such as removing obstructing objects before manipulating the target, ensuring robust execution in complex scenes.

IV. EXPERIMENT SETTING

The update step Δt is chosen as 0.3. c_{min} is set to 0.3. τ is set to 50 pixels. r_i expanded with 10 %. All hyperparameters are selected via a small grid search on a separate tuning set (See supplementary video).

Inputs for human view are collected through the Meta ARIA glasses. The robot view is collected through the Intel Realsense D435i RGBD camera. For manipulation we utilized a Franka Emika Panda 7DOF robot manipulator and various manipulation objects. Multi-modal data processing is performed on a computer equipped with a Nvidia RTX 4080 GPU. All models are deployed using TensorRT for efficient inference. Our Glance-Say operates asynchronously, initiating multi-perspective alignment at the start of interaction and when new objects appear with runtime < 20 ms. The total runtime of the remaining components (including YOLO26) is < 15 ms. In comparison, the frame rate for the eye-tracking camera is 10 FPS and for Ego-RGB camera is 20 FPS.

As shown in Fig. 5, We design four scenarios:

- Scenario 1 (S_1): Users wear Aria glasses. When the targets moving randomly, we evaluate robustness of our algorithm by computing the tracking rate, defined as the ratio between correctly identified intent frames and the total number of detected frames. When the targets remain static, participants continuously attempts to select a specified targets using gaze (including intent changing). A selection is recorded only when the participant explicitly indicates that the intended object has been successfully selected. We evaluate selection accuracy as the ratio between correctly identified selections and the total number of trials. Users maintained a approximately 40 cm from the test plate to obtain relatively accurate gaze points (error ≈ 0.4 cm).
- Scenario 2 (S_2): The glasses are fixed at a user-like position to eliminate head motion effects. We measure object alignment accuracy (Number of correctly aligned objects / Total number of objects) at different distances from the test area and under varying relative viewing angles between the glasses and the robot-mounted camera. To reduce the influence of object detection bias, we use nine visually similar Duplo blocks (3 rows and 3 columns), making the alignment evaluation more challenging and controlled.
- Scenario 3&4 (S_3 & S_4): Users complete predefined manipulation tasks using different interaction methods. We report the task success rate, the command duration (defined as the duration from the start of user command input to the end of command input), and the task duration (defined as the duration from the start of command input to the completion of robot execution).

We recruited 16 participants with upper-limb disabilities from multiple countries, all fluent in English (IRB approved). Each scenario and baseline methods was repeated 10 times per participant. To minimize learning effects, both the scenarios and interaction methods were randomized across trials.

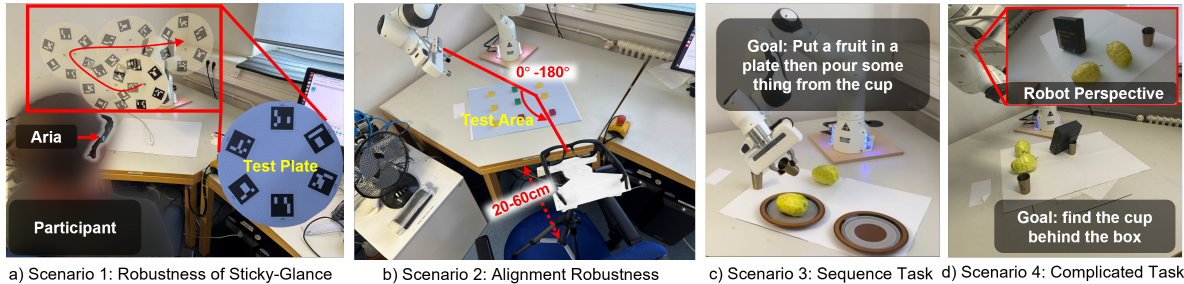


Fig. 5. Overview of Experimental Scenarios. Scenario 1 evaluates robustness of our proposed intent confidence algorithm. Scenario 2 evaluate the robustness of multi-perspective alignment. Scenarios 3-4 assess real-world robotic task execution at increasing complexity. Sequence tasks involve combinations of simple actions such as pick, put, pour, and position swap. Complicated tasks require robots to handle occlusion issues and the overlapping of objects.

V. DISCUSSION

A. Intent Recognition Robustness

Tab. I shows the tracking rate under dynamic motion and the selection accuracy under static conditions in S_1 of different intent recognition baselines. To evaluate intent recognition robustness, we compare our method with state-of-the-art gaze-based intent recognition baselines, including kNN-based [16], fixation-based [6], distribution-based [7], HMM-based [2], and LSTM-based [12] approaches. Methods requiring initialization are not applicable [13].

When targets move randomly, gaze often lags behind the object, causing baseline methods to lose target tracking and resulting in low tracking rates. Under static conditions, fixation-based [6] and kNN-based [16] methods suffer from natural micro-saccades, which can shift gaze outside the object region and reduce accuracy. HMM-based approach [2] improves dynamic scenarios by introducing temporal belief propagation. However, the predefined goal-switching and transition probabilities are difficult to fine-tune. A small switching probability introduces strong inertia in belief updates, leading to delayed intent transitions in static scenarios, whereas a larger switching probability cause belief oscillation and instability in dynamic settings. LSTM-based (and other learning-based) [11], [12] approaches infer intent based on all gaze points within a time window, leading to an ambiguity intent recognition when intent transitions occur.

In contrast, our approach explicitly accumulates geometric distance and directional trends, achieving a tracking rate of 0.92, significantly outperforming all baselines. Our method does not require fixation or predefined goal transition probability and achieves the highest selection accuracy (0.98) with relative small Min. Samples (3).

B. Multi-Perspective Alignment Robustness

Tab. II compares alignment accuracy under varying distances and relative viewing angles. At short distances (40–50 cm), all methods achieve high accuracy. However, as distance increases, ArUco-based [29] alignment degrades due to marker detection loss, and feature-matching methods [3] fail to reliably match features on objects.

TABLE I
INTENT RECOGNITION ROBUSTNESS

Methods	Tracking Rate (Dynamic)	Selection Accuracy (Static)	Min. Samples (Static)
kNN-based [16]	0.22	0.63	1
Fixation-based [6]	0.13	0.84	5
Distribution-based [7]	0.72	0.91	3
HMM-based [2]	0.81	0.79	20
LSTM-based [12]	0.28	0.72	25
Our	0.92	0.98	3

Min. Samples: the minimum number of sampling points required for to recognize intent. HMM-based method need temporal average filter and LSTM-based method can only run with fixed-length time window, result in a large number of sampling points being required.

In contrast, our alignment method remains stable across all tested distances and angles, maintaining above 0.84 accuracy even at 80 cm. This demonstrates strong robustness to viewpoint variation and long-range observation.

C. Task Completeness

We compare our system with representative gaze-based HRI pipelines, as shown in Tab. III. MR-GUI [15] and GlanceGaze [6] both rely on fixation-based object selection. MR-GUI additionally requires fixation on a GUI to choose actions, increasing command duration (18.3s & 5.8s). GlanceGaze infers actions using a VLM, but still depends on repeated fixation for object selection. These repeated fixations lengthen command duration (2.4s) and reduce success rate (0.59) in S_4 , where object overlap makes accurate gaze-based selection difficult. Moreover, GlanceGaze occasionally misinterprets action intent (e.g., confusing put and pour), resulting in lower success rates (0.67) in S_3 . FreeView [1] performs teleoperation through a virtual GUI around the robot end-effector. This requires continuous manual control, leading to extremely long command duration (193.8s & 167.9s) and reduced practicality. FAM-HRI [3] combines weighted gaze clustering with speech for multi-modal interaction, reducing command duration compared to unimodality. However, its intent recognition remains sensitive to overlapping objects, leading to reduced robustness in S_4 (0.73). In contrast, our method achieves the highest success rates and the shortest interaction and task durations.

TABLE II
COMPARISON OF MULTI-PERSPECTIVE ALIGNMENT ROBUSTNESS

Distance (cm)	ArUco [29]			Matching [3]			Our		
	0°	90°	180°	0°	90°	180°	0°	90°	180°
40	1.00	1.00	1.00	1.00	1.00	0.97	1.00	1.00	1.00
50	0.99	1.00	1.00	0.96	0.97	0.94	1.00	1.00	1.00
60	0.78	0.72	0.75	0.84	0.73	0.67	0.98	0.96	0.99
70	0.48	0.52	0.61	0.19	0.21	0.17	0.94	0.91	0.92
80	0.41	0.38	0.32	0.13	0.09	0.11	0.84	0.86	0.89

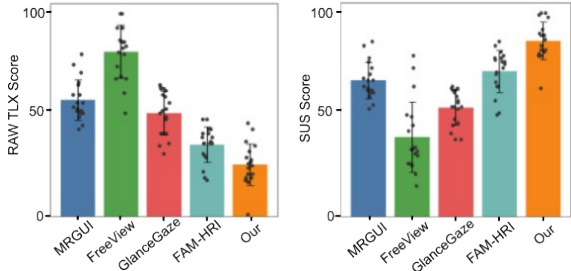


Fig. 6. Final user outcomes for the the raw NASA-TLX (right) and System Usability Score (left).

The sticky-glance algorithm enables robust object selection even in overlapping scenes (0.98 & 0.96), while continuous shared control reduces task duration compared to target pose control (36.4s & 29.5s), reducing task duration for nearly 10 % compared with [3]. The integration of gaze for object grounding and speech for action specification ensures both efficiency and reliability.

D. User Study

After completing all baseline and proposed methods, participants completed a NASA-TLX workload assessment [30] and a System Usability Scale (SUS) [31]. The distribution and summary statistics are shown in Fig. 6 and Tab. IV.

For NASA-TLX results, a Shapiro–Wilk test confirmed that all groups followed normal distribution ($p > 0.05$). Results from ANOVA found significant differences between the groups ($p < 0.05$). Post-hoc Tukey HSD analysis showed that both FAM-HRI and our method yielded significantly lower than other baselines (minimum difference = 15.68, $p < 0.05$), and our method further achieved significantly lower than FAM-HRI (difference = 9.78, $p < 0.05$). These results indicate that incorporating speech reduces cognitive load by explicit action intent, while the sticky-glance algorithm further lowers workload by eliminating the need for prolonged fixation with a short glance.

For SUS results, a Shapiro–Wilk test confirmed that all groups followed normal distribution ($p > 0.05$) except MRGUI ($p = 0.03 < 0.05$). ANOVA found significant differences between the groups ($p < 0.05$). Post-hoc Tukey HSD analysis showed that our method significantly higher than other baselines (minimum difference = 15.05, $p < 0.05$). Participants reported that our interaction paradigm reduces learning effort and improves task success, leading to a clear user preference for the proposed approach.

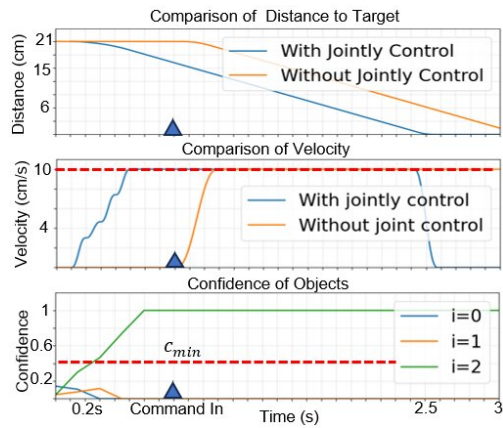


Fig. 7. Ablation Study of Continuous Shared Control

E. Ablation Studies

1) *Continuous Shared Control*: We compare the proposed shared control to target-pose control by analyzing end-effector velocity and distance to the target. As shown in Fig. 7, without shared control, the robot remains stationary until an command is explicit. In contrast, shared control enables continuous pre-command motion toward potential virtual target, reducing the remaining distance for nearly 40% once the command is explicit.

2) *Sticky-Glance Algorithm*: Tab. V evaluates the contribution of e_i^{dist} and e_i^{dir} . Removing any evidence reduces robustness under dynamic motion and static target.

The full model achieves the highest tracking rates across all settings (0.92 under dynamic and 1.0 under static), demonstrating that jointly modeling distance and motion direction is essential for stable intent grounding.

3) *Interaction Modalities*: We evaluate different interaction modalities in S_4 , (participants wearing the glasses). In the test area with 3×3 Duplo blocks, the user is required to grasp a specified block using the robot arm.

As shown in Tab. VI, speech interaction (w.o. Gaze) leads to longer command duration and lower success rates. Commands such as “pick up the brick in the third row, second column” are ambiguous and increase cognitive effort in spatial referencing. Gaze interaction (w.o. Speech) allows efficient object selection, but action selection requires looking at predefined ArUco markers as a GUI, which increases command duration and cognitive load [18].

In contrast, our multi-modal approach achieves the shortest command duration (1.38s) and highest success rate (0.97), demonstrating that combining gaze-based object grounding with speech-based action specification enables more efficient and reliable interaction.

VI. CONCLUSION AND FUTURE WORK

In this work we propose a system for combined glance and speech command input to control a robot arm, providing an efficient method for gaze denoising that enables stable object-level intent grounding and continuous control. The proposed sticky-glance algorithm converts sparse and noisy

TABLE III
COMPARISON OF TASK COMPLETENESS CROSS DIFFERENT GAZE-BASED ROBOT SYSTEM

Methods	Modality	Control	Paradigm	Success rate		Command Duration (s)		Task Duration (s)	
				S_3	S_4	S_3	S_4	S_3	S_4
MR-GUI [15]	Gaze	Target Pose Control	Fixation + GUI in MR	0.93	0.61	18.3	5.8	52.6	34.7
FreeView [1]	Gaze	Teleoperation	Virtual GUI around Robot	-	-	193.8	167.9	-	-
GlanceGaze [6]	Gaze	Target Pose Control	Fixation	0.67	0.59	7.6	2.4	48.7	36.1
FAM-HRI [3]	Gaze+Speech	Target Pose Control	Weighted Gaze & Cluster	0.93	0.73	6.4	1.7	41.6	32.4
Our	Gaze+Speech	Continuous Control	Sticky Glance	0.98	0.96	4.2	1.4	36.4	29.5

To eliminate the influence of different action generators, all baseline methods except the FreeView approach employ similar behavior tree-based planners. The FreeView method is based on teleoperation, therefore success rate is meaningless. Additionally, task duration equates to command duration. No confirmation process is performed in this experiment.

TABLE IV
RESULTS OF USER STUDY

Methods	NASA-TLX ↓	SUS ↑
MR-GUI [15]	57.42±9.96	66.89±9.05
FreeView [1]	81.21±13.14	39.05±17.31
GlanceGaze [6]	51.05±10.91	53.57±8.61
FAM-HRI [3]	35.36±8.71	71.36±10.32
Our	25.57±11.34	86.42±9.29

TABLE VI

ABLATION STUDY OF DIFFERENT MODALITIES

Modality	Command Duration (s)	Success rate
w.o. Gaze	3.48	0.79
w.o. Speech	2.93	0.92
Our	1.38	0.97

TABLE V

ABLATION STUDY OF STICKY-GLANCE ALGORITHM

Methods	Tracking Rate (Dynamic)	Selection Accuracy (Static)
w.o. e_i^{dir}	0.86	0.93
w.o. e_i^{dist}	0.74	0.81
our	0.92	1.00

gaze signals into temporally stable, object-anchored intent, allowing reliable target selection with only a brief glance. By integrating confidence-weighted continuous shared control, the robot proactively maintains readiness while ensuring safe and smooth task execution. Extensive experiments demonstrate strong robustness under dynamic motion, multi-perspective alignment, and overlapping object scenarios. User studies further confirm reduced cognitive load and improved usability compared to representative gaze-based baselines. These results highlight that our system provides an efficient and reliable paradigm for HRI.

Despite the performance gains, our current framework relies on some handcrafted components, which may limit its scalability and generalization across diverse, unstructured environments. Future work will focus on developing a unified end-to-end multimodal model to jointly learn gaze grounding, intent prediction, and action generation, thereby enhancing the system’s adaptability in complex human–robot interaction scenarios.

REFERENCES

- [1] M.-Y. Wang, A. A. Kogkas, A. Darzi, and G. P. Mylonas, “Free-view, 3d gaze-guided, assistive robotic system for activities of daily living,” in *2018 IEEE/RSJ International Conference on Intelligent Robots and Systems (IROS)*, 2018.
- [2] S. Jain and B. Argall, “Recursive bayesian human intent recognition in shared-control robotics,” in *2018 IEEE/RSJ International Conference on Intelligent Robots and Systems (IROS)*, 2018.
- [3] Y. Lai, S. Yuan, B. Zhang, B. Kiefer, P. Li, T. Deng, and A. Zell, “Fam-hri: Foundation-model assisted multi-modal human-robot interaction combining gaze and speech,” 2025.
- [4] M. S. H. Sunny, M. I. I. Zarif, I. Rulik, J. Sanjuan, M. H. Rahman, S. I. Ahamed, I. Wang, K. Schultz, and B. Brahmi, “Eye-gaze control of a wheelchair mounted 6dof assistive robot for activities of daily living,” *Journal of NeuroEngineering and Rehabilitation*, 2021.
- [5] A. Belardinelli, “Gaze-based intention estimation: Principles, methodologies, and applications in hri,” *J. Hum.-Robot Interact.*, 2024.
- [6] T. Y. H. Tay, X. Yan, J. Ouyang, D. Wu, W. Jiang, J. Kao, and Y. Cui, “Intent at a glance: Gaze-guided robotic manipulation via foundation models,” in *Proceedings of the RSS 2025 Workshop on Robot Planning in the Era of Foundation Models (FM4RoboPlan)*, 2025.
- [7] Z. Yin, Z. Wan, M. Yang, Y. Xiong, W. Wang, and S. Wu, “Robust gaze-based intention prediction for real-world scenarios,” *IEEE Transactions on Cognitive and Developmental Systems*, 2024.
- [8] S. Fuchs and A. Belardinelli, “Gaze-based intention estimation for shared autonomy in pick-and-place tasks,” *Frontiers in Neurobotics*, 2021.
- [9] C.-M. Huang and B. Mutlu, “Anticipatory robot control for efficient human-robot collaboration,” in *2016 11th ACM/IEEE International Conference on Human-Robot Interaction (HRI)*, 2016.
- [10] H. Admoni and S. S. Srinivasa, “Predicting user intent through eye gaze for shared autonomy,” in *AAAI fall symposia*, 2016.
- [11] X. Wang, A. Haji Fathaliyan, and V. J. Santos, “Toward shared autonomy control schemes for human-robot systems: Action primitive recognition using eye gaze features,” *Frontiers in Neurobotics*, 2020.
- [12] I. Gonzalez-Diaz, J. Benois-Pineau, J.-P. Domenger, D. Cattaert, and A. de Rugy, “Perceptually-guided deep neural networks for ego-action prediction: Object grasping,” *Pattern Recognition*, 2019.
- [13] B. Yang, J. Huang, X. Chen, X. Li, and Y. Hasegawa, “Natural grasp intention recognition based on gaze in human–robot interaction,” *IEEE Journal of Biomedical and Health Informatics*, 2023.
- [14] Y. Shi, Y. Yan, Z. Li, C. Liang, Y. Wang, C. Yu, and Y. Shi, “Casualgaze: Towards modeling and recognizing casual gaze behavior for efficient gaze-based object selection,” *arXiv:2408.12710*, 2024.
- [15] J. D. P. Prada, M. H. Lee, and C. Song, “A gaze-speech system in mixed reality for human-robot interaction,” in *2023 IEEE International Conference on Robotics and Automation (ICRA)*, 2023.
- [16] S. Jiang, W. Zhang, J. Liu, H. Li, Z. Wang, Y. Zhou, and B. He, “A novel human-in-the-loop multimodal intention fusion method for human-robot interaction,” *IEEE Transactions on Automation Science and Engineering*, 2025.

- [17] A. D. Dragan and S. S. Srinivasa, "A policy-blending formalism for shared control," *The International Journal of Robotics Research*, 2013.
- [18] E. N. Sardinha, N. Zook, V. R. Garate, D. Western, and M. Munera, "Comparison of three interface approaches for gaze control of assistive robots for individuals with tetraplegia," in *2025 IEEE International Conference on Robotics and Automation (ICRA)*, 2025.
- [19] X. Wang and V. J. Santos, "Gaze-based shared autonomy framework with real-time action primitive recognition for robot manipulators," *IEEE Transactions on Neural Systems and Rehabilitation Engineering*, 2023.
- [20] Y. Mansour, A. Savio Fernandes, K. Somasundaram, T. Hefny, M. Shakeri, O. V. Komogortsev, A. Sharma, and M. J. Proulx, "Enabling eye tracking for crowd-sourced data collection with project aria," *IEEE Access*, 2025.
- [21] G. Jocher, J. Qiu, A. Chaurasia, and contributors, "Ultralytics yolo," 2026, accessed: 2026-03-05. [Online]. Available: <https://github.com/ultralytics/ultralytics>
- [22] Y. Zhang, P. Sun, Y. Jiang, D. Yu, F. Weng, Z. Yuan, P. Luo, W. Liu, and X. Wang, "Bytetrack: Multi-object tracking by associating every detection box," in *European conference on computer vision*, 2022.
- [23] Y. Wu, Y. Zhang, D. Zhu, Z. Deng, W. Sun, X. Chen, and J. Zhang, "An object slam framework for association, mapping, and high-level tasks," *IEEE Transactions on Robotics*, 2023.
- [24] H.-S. Fang, C. Wang, H. Fang, M. Gou, J. Liu, H. Yan, W. Liu, Y. Xie, and C. Lu, "Anygrasp: Robust and efficient grasp perception in spatial and temporal domains," *IEEE Transactions on Robotics (T-RO)*, 2023.
- [25] P. Lindenberger, P.-E. Sarlin, and M. Pollefeys, "Lightglue: Local feature matching at light speed," in *Proceedings of the IEEE/CVF International Conference on Computer Vision (ICCV)*, 2023.
- [26] T. D. Barfoot, *State estimation for robotics*. Cambridge University Press, 2024.
- [27] J. Hu, Z. Jiang, X. Ding, T. Mu, and P. Hall, "Vgpn: Voice-guided pointing robot navigation for humans," in *2018 IEEE International Conference on Robotics and Biomimetics (ROBIO)*, 2018.
- [28] J. Chen, S. Xiao, P. Zhang, K. Luo, D. Lian, and Z. Liu, "Bge m3-embedding: Multi-lingual, multi-functionality, multi-granularity text embeddings through self-knowledge distillation," 2023.
- [29] D. Weber, E. Kasneci, and A. Zell, "Exploiting augmented reality for extrinsic robot calibration and eye-based human-robot collaboration," in *2022 17th ACM/IEEE International Conference on Human-Robot Interaction (HRI)*, 2022.
- [30] J. Brooke *et al.*, "Sus-a quick and dirty usability scale," *Usability evaluation in industry*, 1996.
- [31] S. G. Hart and L. E. Staveland, "Development of nasa-tlx (task load index): Results of empirical and theoretical research," in *Advances in psychology*. Elsevier, 1988.